Quality control of laser welds based on the weld surface and the weld profile

Julia Hartung[1,2], Andreas Jahn[2], and Michael Heizmann[1]

[1] Karlsruhe Institute of Technology, Institute of Industrial Information Technology, Hertzstraße 16, 76187 Karlsruhe, Germany
[2] TRUMPF Laser GmbH, Aichhalder Str. 39, 78713 Schramberg, Germany

Abstract 2D or 3D sensor technology can be used for data acquisition to monitor the weld quality during laser welding. Compared to a 2D camera image, the 3D height data contains additional relevant information for quality inspection. However, the disadvantages are system complexity, higher costs, and longer acquisition times. Therefore, we compare two image-based methods with the quality assessment based on height data. The first method uses feature vectors of coaxial acquired grayscale images. The significant advantage is that a camera is often integrated into the laser system, so no additional hardware is required. In the second approach, we use an AI-based single-view 3D reconstruction method. The height profile is calculated from a camera image and used for further quality assessment. Thus, we combine the advantages of 2D data acquisition with higher accuracy in evaluating 3D data. In this paper, we analyze a dataset of welded hairpins with different defect types and compare the quality assessment using the height data acquired with OCT, the feature vectors from the camera images, and the reconstructed height data.

1 Introduction

With the substantial increase in automation of industrial production lines, reliable and also automated quality control is essential. Laser

welding processes are a key technology for many industrial applications and must fulfill high-quality requirements [1]. However, various influencing factors can lead to defects in the weld seam, which can impair the quality and functionality of the product and result in safety-relevant defects [2, 3]. Therefore, the companies use strict criteria for welding quality.

An increasingly important application with high-quality requirements for laser welding comes from e-mobility. E-mobility will become more and more prevalent in individual transportation in the future. This is why vehicles' designs and various components are constantly refined and optimized. For the new generation of motors, automotive manufacturers increasingly use stators with so-called hairpin technology. The conventional copper windings in the stator of an electric motor are replaced by thick copper rods that are welded together, which saves space and improves the efficiency of an electric motor. Depending on the motor design, between 160 and 220 pairs of copper bars are inserted into the sheet metal stacks of a stator, and the ends are connected, usually by laser welding [4–6]. To ensure the high quality of the entire stator, each weld must be checked for a defect [5, 7]. Different properties and measured variables can be used to evaluate the quality of the weld seam [7, 8]. Various works show that the evaluation of three-dimensional data provides higher accuracy than the analysis of two-dimensional camera images [8–10]. The disadvantages are higher hardware costs, system complexity, and longer process times.

This work presents an approach that computes the height map from a camera image instead of acquiring it with a 3D sensor. This procedure allows us to use the height data for quality assessment without the disadvantages mentioned above. We perform the 3D reconstruction algorithm using a convolutional neural network [11]. The rest of this paper is organized as follows: Section 2 discusses the state of research in welding quality evaluation of hairpins and using a 3D reconstruction algorithm. Section 3 describes the experimental setup and investigations of the generated dataset. Building on this, section 4 introduces different approaches for predicting the hairpin quality from image data, 3D data, and reconstructed 3D data. In section 5, the results are discussed before section 6 provides a summary as well as an outlook for future research activities.

2 Related work

There are a variety of quality monitoring and control systems for laser welding. The use of machine learning (ML) methods is evaluated in [12] and [7]. Unlike many ML applications, the amount of data samples in the industrial environment, especially in research, is limited, and the computing time may not extend the production time [13].

In [14] a post-inspection of laser welds is performed based on images using semantic segmentation. Here, a tiny network structure is used for the reasons just mentioned. [7] uses images from 3 perspectives, front, top and back, to evaluate the seam quality of hairpins. More information about the seam connection can be obtained through the different views. However, integration into a production line is more complex because it is often difficult to attach cameras to the side. The resulting accuracy of the network is in the range from 61% to 92% [7]. [8] analyze and compare different Convolutional Neural Networks (CNN) to perform post-process quality control of hairpins. In addition to 2D grayscale images, 3D scans are used as input to the CNN. Based on the 3D scans, the classification accuracy is higher than using the 2D images. This result supports the assumption that the height values contain relevant information for quality assessment. In [15] and [10], a height profile is also used to determine weld quality in laser welding. Especially in hairpin welding, the height difference between the pair of hairpins before and after welding provides information about the volume of the molten material. This volume, together with the other measured parameters of the surface profile of the weld, is crucial for the welding quality of the hairpins [9].

Due to the cost, higher system complexity and acquisition time, it is advantageous to calculate the height profile using a method of 3D reconstruction. [16] use shape from shading (SFS) to perform a 3D reconstruction of a weld seam. Based on the curvature features, the weld quality is evaluated. Especially in the classification task of complex welds with complex structures and characteristics, the curvature feature contains limited information and cannot be applied to this task. The SFS algorithm reconstructs a shape based on shading variation, assuming a single point light source and Lambertian surface reflectance, where the brightness of an image pixel depends on the light source direction and the surface normal. Due to the hairpins' height and the
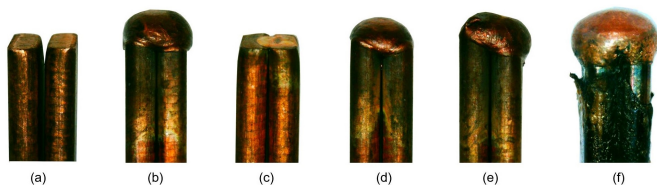
Figure 1: Welding results of hairpins. (a) no weld, (b) good weld, (c) pin not in the focus of the laser, (d) weld with too low power, (e) misaligned pin pair, (f) insulated copper rods.

welding bead's dome, a reconstruction from a single image with SFS is impossible since the incidence of light can only be realized on one side and the other side is accordingly in shadow. [17] calculates a 3D reconstruction from several images taken with different relative positions between camera and weld during the data acquisition phase. Based on the resulting 3D model, a quality evaluation of the weld is performed.

Deep learning-based methods for 3D reconstruction have shown promising results in various research fields. While classical methods deal with shape and image properties such as reflection, albedo, or light distributions, deep learning-based methods use complex network architectures to learn the correlations between 2D and 3D data. Many approaches are challenging to integrate into existing industrial processes because new cameras or illumination equipment are required. [11] compare different single-image reconstruction methods on an industrial dataset. In their investigations, a variation of the U-Net, the stacked dilated U-Net (SDU-Net), has prevailed with its performance.

3 Material

Laser-welded pairs of copper pins, as shown in Figure 1, are used for data acquisition. Different welding results are recorded to obtain a representative data set that includes error cases. Data from 953 hairpins were acquired from a position above the pins, as this perspective allows the integration with the existing industrial process. The 2D intensity images of the hairpins were captured using a Baumer VCXG-15M.I industrial camera based on CMOS technology. An optical coherence tomography (OCT) scanner from Lessmüller Lasertechnik is used to
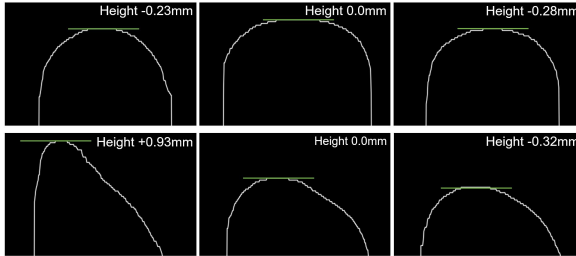
Figure 2: OCT scans at different positions (left side, center, right side). Top row - similar height values indicate a good seam. Bottom row - the different heights indicate the fault case (misaligned pin pair).

capture the 3D data. Many line scans are performed to obtain the height maps of the entire weld. These are then combined to create an overall height map of the component. The exact structure of the data acquisition and the assignment of the camera data to the height data is explained in detail in [11]. To reflect the real situation in the industry with low data availability, we use 10% of the data, i.e., 95 samples, for algorithm development. The other 90%, i.e., 858 samples, are used for testing and evaluation.

4 Detection of weld quality

To compare the result of quality assessments, we analyze various input data for the weld inspection. We use the height data acquired by the OCT, camera images, and reconstructed height data to create feature vectors.

4.1 Height data acquired with OCT

The OCT sensor measures the relative height differences within the weld seam. Good welding of a pin pair results in a round welding bead, which has its maximum in the center. The line scans should have a structure like the upper row in Figure 2 over the entire weld bead. The bottom row shows the images at the same positions of a weld with misaligned pins for comparison. As in [18] and in [19], we compare
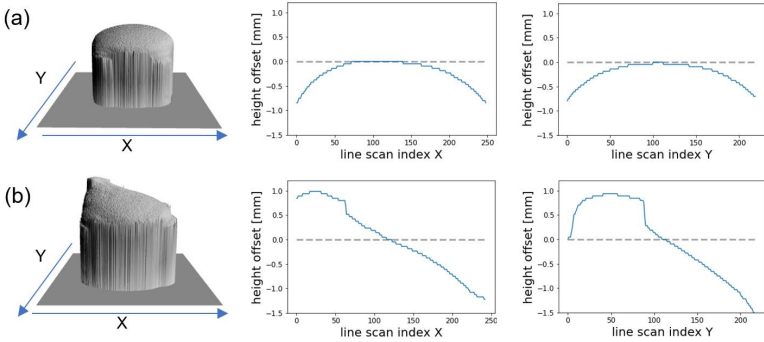
Figure 3: Difference of the maximum values of the line scans to the center. The maximum value of each line scan is determined. The difference to the center is calculated and the values are plotted in a curve. Mathematically this means $f(l_i) = |h_c - \max l_i|$, where l_i is the line scan with index i and h_c is the height value in the center. (a) Good welds result in a curve with its maximum in the center. (b) Defective welds, such as misaligning pins or pins that are not in the laser's focus, can be detected in the curve.

multiple line scans with each other. For higher accuracy, we scan the hairpin in the x- and y-directions with lines at distances of 18 μm.

For quality assessment, we use different criteria. Analogous to [18], we consider the difference between the maximum height values of the individual line scans to the height of the pin center. Through this comparison, we can detect misalignment of the hairpins or misshapen welding beads. The procedure is visualized in Figure 3. In addition to the curve profile, we evaluate the line scans' maximum and minimum distance to the pin center's height. If the distance to the pin center is too small, the weld is not sufficiently stable. If, on the other hand, the minimum distance is too large, this provides information about pores or cracks in the pin surface. We also consider the width of the weld bead in the evaluation.

4.2 Camera images

As mentioned earlier, it is not always possible to capture the height profile due to time constraints and the increasing cost and complexity of the system. Therefore, we develop a different approach by deriving
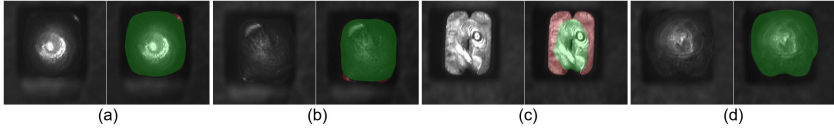
Figure 4: Detection of the welded and unwelded pin surface in the camera image. The detection of the surface of the weld, as well as the unwelded pins, is shown. In each case, the right image shows the binary mask overlaid on the image (green - weld, red - unwelded pin). (a) good weld, (b) misaligned pin pair, (c) pin not in the focus of the laser, (d) insulated copper rods.

the quality-relevant properties of the weld from the grayscale image. As with OCT scans, we can also infer the width of the weld from the grayscale image. In addition, the size of the weld surface provides information about the stability of the weld. We can also detect this size in 2D images. For the detection of the seam area, threshold-based methods reach their limits due to the low-intensity differences and contrasts in the images. However, CNN-based semantic segmentation can detect the area well, even in small network architectures. Analogous to [6], we train a small SDU-Net to detect both the welded seam and the non-welded pin regions. The predicted masks are shown in an overlay representation in Figure 4.

We can already detect many defect cases by evaluating the width of the weld and the size of the two classified areas. As a further evaluation, we analyze the shape of the weld. In good welds, this is approximately circular and has no solid corners and edges. However, if too little material is melted during welding, no round weld bead is formed, and the contour is slightly angular due to the pin shape. Other defects, such as copper pins that have not had their insulation stripped, also result in edges in the weld shape. Since the weld surface is a closed contour, Fourier descriptors can be used to characterize it. Analogous to [20], we compute the Fourier descriptors of the contours. An evaluation of the harmonics considers the complexity of the contour. In particular, in combination with the information about the size of the non-welded pin region, this contains information about insufficiently welded pin pairs. The relationship between the defined features and the evaluation result of the seam quality based on the height profile is shown in Figure 5.
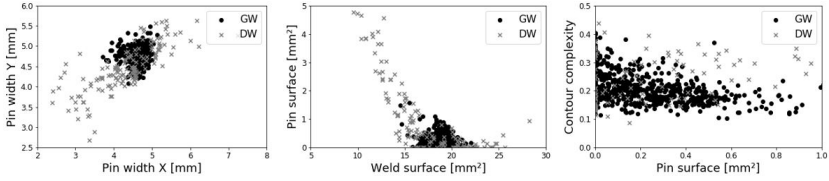
Figure 5: Quality-related features derived from the grayscale images. The correlation of the features derived from the 2D image with the seam quality based on the height profile is shown (GW -good weld, DW - defective weld).

4.3 Height data from the 3D reconstruction algorithm

In the third approach, we use an AI-based single-view reconstruction method. Thus we combine the advantages of the two methods just presented. This approach calculates the height profile from the captured camera image. For this purpose, only one camera image must be taken in the production line, and the algorithm can replace the time-consuming OCT scan. Further analyses can still be performed on the more informative height profile. We use a modified SDU-Net architecture for the reconstruction. Since the model is tiny, with only 162,423 parameters, it can also be executed efficiently on industrial hardware. The exact implementation, the training parameters and the result analysis with deviations from ground truth are explained in detail in [11].

5 Results and discussion

The quality assessment of the 858 test samples is performed separately with each method to evaluate the different approaches. The ground truth is the division into good weld (GW) and defective weld (DW) based on the features derived from the entire recorded height map using OCT. We evaluate the quality assessment based on the criteria visible in the camera image (Cam) and the AI-based 3D reconstruction (3D-R) data. When height data is used for quality assessment, only a few line scans are usually acquired due to time constraints. The scanner made by Lessmueller Lasertechnik has a scan frequency of 70 kHz, so a scan of the entire component takes considerable time. Therefore, we use an approach in which only six OCT scan lines (three in the x-

direction and three in the y-direction) are considered in the evaluation (6L). One scan is in the center of the weld, and the other two are on each side. In another investigation, we only consider the three scans in the x-direction in our evaluation (3L). The feature vectors for the quality assessment are defined based on those of the entire height map. The results are presented in Figure 6 using a confusion matrix.

The AI-based 3D reconstruction using the camera images gives the best results of the four methods compared. 842 of the 858 test samples are classified in the same way as with the ground truth data, even if only the camera image was used as input. The discrepancies are due to borderline cases. As described in detail in [11], the model trained on 95 images has an average deviation of 93.5 µm from the ground truth. Due to the rule-based partitioning into GW and DW, in case of doubt, the deviation from one pixel value may yield a different result. One pixel value corresponds to a deviation of 46.8µm in height and a difference of 18µm in width. The borderline cases are welds where the width or the minimum height of the weld bead was barely reached with one method and just missed with the other.

When evaluating the results based on the camera images, it is noticeable that more pin pairs with height offset were detected as GW. This wrong classification can be attributed to the fact that the height offset is not considered in any of the used image-based classification features. The offset cannot be identified by the shape, size of the weld bead or the area of the unwelded pin surface. Therefore, this error case unfortunately often remains undetected. On the other hand, samples that are incorrectly classified as DW can be attributed to tiny weld beads. If less material was melted during the process, the welds often have a rather rectangular shape due to the pin shape. In some cases, the height of the weld is sufficient to create a stable weld, although it still has an edged shape. Based on the camera image, these samples are classified as DW because they look very similar to the unstable low-power welds. GWs with a round weld bead are reliably detected as GWs.

The evaluation with a few line scans also shows more deviating results than the evaluation with 3D reconstruction. In addition to borderline cases, these methods incorrectly classify pin pairs in which one of the pins was only partially connected or welds with spatter as GW. Especially when evaluating with only three scans in the x-direction, insufficiently welded pins (e.g. Figure 1(c, d)) were missed more often.

OCT GW	679	20	OCT GW	694	5	OCT GW	691	8	OCT GW	688	11
OCT DW	25	134	OCT DW	11	148	OCT DW	35	124	OCT DW	20	139
	Cam GW	Cam DW		3D-R GW	3D-R DW		3L GW	3L DW		6L GW	6L DW

Figure 6: **Comparison of the results of the different methods.** The results of the approaches: Camera image (Cam), AI-based 3D reconstruction (3D-R), six line scans OCT (6L) and three line scans OCT (3L) are compared with ground truth based on the features from the entire height map.

6 Conclusion

We have developed and compared different methods for quality assessment in hairpin welding. In addition to analyzing the acquired height profile, we have successfully determined the quality based on a grayscale image. For the image-based evaluation, we used two different approaches. First, we used features derived from the image, such as the width and shape of the weld, to perform a quality assessment. The most significant deficiencies were pin pairs, which have an offset between the pins. This misalignment is not captured in the image-based features and, thus, is not considered in the quality assessment. With this approach, the misalignment would have to be checked and corrected before welding, completely avoiding the faulty weld. The significant advantage of using the image-based features is that no additional height scanner is needed, which reduces cost, setup effort, and acquisition time and allows quality analysis through a software update. The calculation of the binary mask following the approach of [6] only requires 16 ms on an i5-7300U CPU. It can be integrated into the process with the subsequent algorithmic evaluation without additional hardware requirements. In a second approach, we performed an AI-based 3D reconstruction on a single grayscale image and then used the computed height data for quality assessment. With this approach, we achieved higher accuracy and could correctly assign the test samples, except for some borderline cases. The approach presented in [11] allows reconstruction based on a single grayscale image. For this purpose, a small SDU-Net architecture is used, which can be executed on an i5-7300U CPU in only 45 ms. This method opens up a new pos-

sibility for quality evaluation. Unlike feature-based evaluation of the camera image, a height scanner is required to train the AI model. Afterward, however, only one camera image is needed in the productive system, and the time for the height scan can be saved.

In future work, we will integrate the developed solutions into the manufacturing process and evaluate the results on other components than hairpins. In addition, the robustness and transferability of an AI model for calculating the height profile between different plants will be further investigated. Depending on the results, it might be necessary to improve the networks or the algorithms used downstream for quality assessment.

References

1. M. Jäger, S. Humbert, and F. A. Hamprecht, "Sputter tracking for the automatic monitoring of industrial laser-welding processes," *EEE Trans. Ind. Electron*, vol. 55, no. 5, pp. 2177–2184, 2008.

2. M. Zhang, G. Chen, Y. Zhou, S. Li, and H. Deng, "Observation of spatter formation mechanisms in high-power fiber laser welding of thick plate," *Appl. Surf. Sci.*, vol. 280, pp. 868–875, 2013.

3. A. Kaplan and J. Powell, "Laser welding: The spatter map," *29th Int. Congr. on Appl. of Lasers and Electro-Optics (ICALEO)*, vol. 103, pp. 683–690, 01 2010.

4. T. Ishigami, Y. Tanaka, and H. Homma, "Development of motor stator with rectangular-wire lap winding and an automatic process for its production," *Electr. Eng. JPN.*, vol. 187, no. 4, pp. 51–59, 2014.

5. T. Glaessel, J. Seefried, and J. Franke, "Challenges in the manufacturing of hairpin windings and application opportunities of infrared lasers for the contacting process," in *7th Int. Elec. Drives Prod. Conf. (EDPC)*, 12 2017, pp. 1–7.

6. J. Hartung, A. Jahn, O. Bocksrocker, and M. Heizmann, "Camera-based in-process quality measurement of hairpin welding," *Appl. Sci.*, vol. 11, no. 21, p. Art.Nr. 10375, 2021.

7. A. Mayr, B. Lutz, M. Weigelt, T. Gläßel, D. Kißkalt, M. Masuch, A. Riedel, and J. Franke, "Evaluation of machine learning for quality monitoring of laser welding using the example of the contacting of hairpin windings," in *8th Int. Elec. Drives Prod. Conf. (EDPC)*, 2018, pp. 1–7.

8. J. Vater, M. Pollach, C. Lenz, D. Winkle, and A. Knoll, "Quality control and fault classification of laser welded hairpins in electrical motors," in *2020 28th Eur. Signal Process. Conf. (EUSIPCO)*, 2021, pp. 1377–1381.

9. N. Deyneka-Dupriez, "Implementing oct for industrial weld monitoring," *Laser Syst. Europe*, 09 2019.

10. C. Stadter, M. Schmoeller, M. Zeitler, V. Tueretkan, U. Munzert, and M. F. Zaeh, "Process control and quality assurance in remote laser beam welding by optical coherence tomography," *J. Laser Appl.*, vol. 31, no. 2, 2019.

11. J. Hartung, P. M. Dold, A. Jahn, and M. Heizmann, "Analysis of AI-based single-view 3D reconstruction methods for an industrial application," *Sensors*, vol. 22, no. 17, 2022.

12. A. Mayr, M. Weigelt, M. Masuch, M. Meiners, F. Hüttel, and J. Franke, "Application scenarios of artificial intelligence in electric drives production," *Procedia Manuf.*, vol. 24, pp. 40–47, 2018.

13. M. Weigelt, A. Mayr, J. Seefried, P. Heisler, and J. Franke, "Conceptual design of an intelligent ultrasonic crimping process using machine learning algorithms," *Procedia Manuf.*, vol. 17, pp. 78–85, 2018.

14. J. Hartung, A. Jahn, M. Stambke, O. Wehner, R. Thieringer, and M. Heizmann, "Camera-based spatter detection in laser welding with a deep learning approach," in *Forum Bildverarbeitung 2020*. KIT Scientific Publishing, 2020.

15. G. Ye, J. Guo, Z. Sun, C. Li, and S. Zhong, "Weld bead recognition using laser vision with model-based classification," *Robot. Comput. Integr. Manuf*, vol. 52, pp. 9–16, 2018.

16. Y. Lei, E. Li, T. Long, J. Fan, Y. Mao, Z. Fang, and Z. Liang, "A welding quality detection method for arc welding robot based on 3d reconstruction with sfs algorithm," *J. Adv. Manuf. Technol.*, vol. 94, pp. 1–12, 01 2018.

17. P. Rodríguez-Gonzálvez, M. Rodríguez-Martín, L. F. Ramos, and D. González-Aguilera, "3d reconstruction methods and quality assessment for visual inspection of welds," *Autom. Constr.*, vol. 79, pp. 49–58, 2017.

18. Lessmueller, "Hairpin welding," accessed: 2022-09-01. [Online]. Available: https://lessmueller.de/tasks/harpin-schweissen/?lang=en

19. M. Baader, A. Mayr, T. Raffin, J. Selzam, A. Kühl, and J. Franke, "Potentials of optical coherence tomography for process monitoring in laser welding of hairpin windings," in *11th Int. Elec. Drives Prod. Conf. (EDPC)*, 2021, pp. 1–10.

20. F. P. Kuhl and C. R. Giardina, "Elliptic fourier features of a closed contour," *Comput. graph.*, vol. 18, no. 3, pp. 236–258, 1982.